PCCP

COMMUNICATION

View Article Online
View Journal | View Issue

Cite this: *Phys. Chem. Chem. Phys.*, 2017, **19**, 20338

Received 24th May 2017,
Accepted 6th July 2017

DOI: 10.1039/c7cp03493h

rsc.li/pccp

A reaction model on the self-assembly process of octahedron-shaped coordination capsules†

Yoshihiro Matsumura,[a] Shuichi Hiraoka [b] and Hirofumi Sato *[ac]

Herein, the self-assembly process of an octahedron-shaped coordination capsule was analyzed based on a master equation approach using a reaction network model. This model was found to adequately reproduce the overall experimentally observed time evolutions and enabled us to trace the real-time evolution of transient intermediates, ranging from milli-second to hours. The time evolution of the distribution of individual intermediates species was obtained; a few linear-oligomers located near the reactant were produced at first, followed by an explosive increase in several types of intermediates. All of them were then consolidated into a few species just before the formation of the final product. A long-lived $[Pd_6\mathbf{1}_8Py]^{12+}$ is a key compound, which acts as a kinetic trap in the reaction dynamics.

Introduction

Molecular self-assembly is a fundamental process in both nature and materials science.[1,2] The ultimate goals in this field are the understanding and control of the self-assembly process to elaborate well-defined self-assemblies with desired functions at will. However, to date, only the final products have drawn attention presumably because of the difficulty in the detection of intermediates. Recently, Hiraoka and his co-workers have proposed a novel experimental approach called *n*–*k* analysis to examine the time evolution of the coordination self-assembly process.[3a,b] They have applied this method to the self-assembly of octahedron-shaped coordination capsules, $[Pd_6L_8]^{12+}$ (eqn (1)), which are a typical example of metal-directed self-assembly.[3c,4,5]

$$6[PdPy_4]^{2+} + 8L \rightarrow [Pd_6L_8]^{12+} + 24Py \quad (1)$$

where L is the tritopic ligand (**1**) shown in Fig. 1 and Py denotes pyridine, a monodentate ligand coordinating to the metal center of the metal source. As the metal source can be traced by the ^{1}H NMR signals of Py on $[PdPy_4]^{2+}$, it is possible to quantify all the materials in eqn (1); this enables us to follow the time evolution of the average composition of all the intermediates produced during the self-assembly, $[Pd_a\mathbf{1}_bPy_c]_{av}^{2a+}$, to clarify the self-assembly process even if the intermediates cannot be observed *via* spectroscopy, which is often the case with molecular self-assembly.

From the average numbers a_{av}, b_{av}, and c_{av}, the following parameters $\langle n \rangle$ and $\langle k \rangle$ were calculated and the time variation of ($\langle n \rangle$, $\langle k \rangle$) provided information about the self-assembly process. *n* represents the mean number of metal ions attached

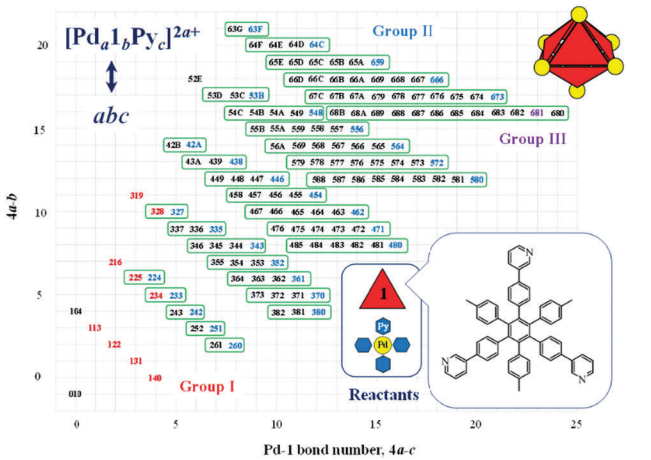

Fig. 1 A map of the 155 chemical species considered, $[Pd_a\mathbf{1}_bPy_c]^{2a+}$, except Py ($a$ = b = 0). a, b, and c are the number of Pd, **1**, and Py, respectively with hexadecimal notation (A = 10, B = 11, C = 12, D = 13, E = 14, F = 15 and G = 16). In this map $[Pd_a\mathbf{1}_bPy_c]^{2a+}$ is denoted as *abc* for clarity. The green enclosures indicate sets of the same *ab*, in which each species is connected through intramolecular ligand exchange with release or inclusion of Py.

[a] *Department of Molecular Engineering, Kyoto University, Kyoto 615-8510, Japan. E-mail: hirofumi@moleng.kyoto-u.ac.jp*
[b] *Department of Basic Science, Graduate School of Arts and Sciences, The University of Tokyo, 3-8-1 Komaba, Meguro-ku, Tokyo, Japan*
[c] *Elements Strategy Initiative for Catalysts and Batteries, Kyoto University, Kyoto 615-8510, Japan*

† Electronic supplementary information (ESI) available: Enumeration procedure for the isomers, a brief explanation of the master equation method, computational details and the analysis for the deuterium system (L = **2**). See DOI: 10.1039/c7cp03493h

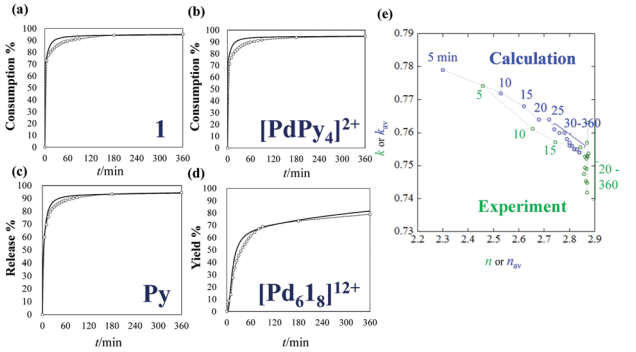

Fig. 2 A comparison between the calculations (solid lines) and experimental results (circles), (a) consumption rate of **1**, (b) the consumption rate of $[PdPy_4]^{2+}$, (c) the release rate of Py and (d) the yield of $[Pd_6\mathbf{1}_8]^{12+}$. (e) *n*,*k*-Analysis obtained by the calculations (blue circles) and experimental results (green circles).

to the tritopic ligand and k represents the ratio of the metal ions attached to the tritopic ligand.[3a]

$$\langle n\rangle = \frac{4a_{\mathrm{av}} - c_{\mathrm{av}}}{b_{\mathrm{av}}}, \quad \langle k\rangle = \frac{a_{\mathrm{av}}}{b_{\mathrm{av}}}$$

For the $[Pd_6\mathbf{1}_8]^{12+}$ capsule, *n*–*k* analysis revealed that the final stage of the capsule formation, $[Pd_6\mathbf{1}_8Py]^{12+} \rightarrow [Pd_6\mathbf{1}_8]^{12+}$ + Py, was the rate-determining step (Fig. 2). Although the *n*–*k* analysis is powerful, an intrinsic disadvantage of this method is the impossibility of providing information on the evolution of the individual intermediates.

Theoretical or computational approaches[6–8] are potentially useful to provide detailed information of the intermediates. However, there are serious difficulties in applying these approaches to molecular self-assembly. In most cases, self-assembly takes place on a time scale of hours or longer, producing a vast number of transiently produced intermediates through various pathways. Therefore, it is almost impossible to compute realistic time evolution of the entire assembly process by simply using molecular dynamics simulations.

An approach utilizing a master equation is a promising way to overcome these difficulties.[9–11] The master equation is capable of describing the time evolution of a chemical reacting system by taking into account the stochastic nature of a large number of chemical species,[9] which cannot be described by the deterministic traditional rate equation.[12] Remarkable differences between the results obtained from the master equation and those obtained from the rate equation were pointed out for a self-assembly system comprising a finite number of molecules.[10] Both approaches and their combination have been applied to relatively simple biochemical reactions,[13–15] gas phase chemical reactions,[16,17] and more complicated self-assembly of virus capsids.[18,19] Note that because of approximation in the rate equation approach, the distributions of the intermediates and final states are shown to become different as compared to those obtained *via* the master equation approach. The difference may be especially important to examine the individual intermediates including the transient intermediates with relatively small populations.

In this study, we have constructed a reaction model to describe the self-assembly process of octahedron-shaped coordination capsules. The time evolutions of the distributions of all the chemical species including intermediates were computed *via* solving a master equation for the reaction model. Herein, we searched for a simple reaction model combining many elementary reaction steps, through which coordination self-assembly generally takes place. As shown below, the present reaction model adequately reproduces the overall time evolutions observed experimentally although some discrepancies arise from the neglect of the detail aspects. The self-assembly process including the intermediates were further quantitatively analyzed.

Reaction model

According to the experimental results,[3a] all the intermediates considered herein were parts of the capsule structure ($1 \le a \le 6$) connected by coordination bonds, and more than 170 000 structures were obtained, which were then categorized based on their composition (see the ESI† for more detail). Herein, 155 species with different compositions, $[Pd_a\mathbf{1}_bPy_c]^{2a+}$, were connected by adding or removing Py or **1** or $[PdPy_4]^{2+}$, as displayed in Fig. 1. Starting from the lower left $[Pd_0\mathbf{1}_1Py_0]$ ("010"), the reaction proceeds towards the upper right direction. The final product $[Pd_6\mathbf{1}_8]^{12+}$ is represented as 680.

All the elementary reactions were categorized into four types of ligand exchange reaction; (i) intermolecular Pd–**1** bond formation between $[Pd_a\mathbf{1}_bPy_c]^{2a+}$ ($b \neq 0$) and **1**, $[Pd_a\mathbf{1}_bPy_c]^{2a+}$ + **1** $\rightarrow [Pd_a\mathbf{1}_{b+1}Py_c]^{2a+}$ + Py, (ii) intermolecular Pd–**1** bond formation between $[Pd_a\mathbf{1}_bPy_c]^{2a+}$ and $[Pd_{a'}\mathbf{1}_{b'}Py_{c'}]^{2a'+}$ except (i), $[Pd_a\mathbf{1}_bPy_c]^{2a+}$ + $[Pd_{a'}\mathbf{1}_{b'}Py_{c'}]^{2a'+} \rightarrow [Pd_{a+a'}\mathbf{1}_{b+b'}Py_{c+c'-1}]^{2(a+a')+}$ + Py ($a \neq 0$ and $a' \neq 0$ or $b = 0$), (iii) the back reaction of (i) and (ii), and (iv) intramolecular Pd–**1** bond formation, $[Pd_a\mathbf{1}_bPy_c]^{2a+} \rightarrow [Pd_a\mathbf{1}_bPy_{c-1}]^{2a+}$ + Py. In the experiment, although the intramolecular ligand exchange, $[Pd_6\mathbf{1}_8Py]^{12+} \rightarrow [Pd_6\mathbf{1}_8]^{12+}$ + Py, was the rate-determining step, none of the species besides those above mentioned in eqn (1) was observed by ^{1}H NMR measurement. Considering the fact that $[Pd_6\mathbf{1}_8Py]^{12+}$ has no isomers with different connections between Pd and **1**, the slow dynamic equilibrium between conformational isomers of $[Pd_6\mathbf{1}_8Py]^{12+}$ is highly anticipated to explain the disappearance of their ^{1}H NMR signals. Based on this idea, two isomers of $[Pd_6\mathbf{1}_8Py]^{12+}$ were considered for our analysis. Although the specific features in the self-assembly process should vary from system to system, the present approach properly describes the general features of the assembly and is expected to be applicable to other self-assembly systems.

In the master equation study, a set of numbers for all the chemical species A (N_A) was introduced to represent a state of the system,

$$\{N\} \equiv \{N_{PdPy_4}, N_{\mathbf{1}}, \ldots, N_{Pd_a\mathbf{1}_bPy_c}, \ldots, N_{Pd_6\mathbf{1}_8}\}$$

In other words, a vector consisting of 156 elements was considered. The probability distribution function of the state $\{N\}$ at time t was defined as $P(\{N\}, t)$,[10] and the amount of

chemical species[3a] at time t was calculated as the mean number using $P(\{N\}, t)$,

$$\langle N_A(t)\rangle = \sum_{\{N\}} N_A P(\{N\}, t)$$

The time evolution was described using the master equation on $P(\{N\}, t)$. It should be emphasized that the present master equation-based approach provides a microscopic description of the reaction, which is totally different from the conventional rate equation. For details of the computational method and further discussion, see the ESI.†

Results and discussion

Fig. 2a–d shows the consumption rates of reactant ($[PdPy_4]^{2+}$ and **1**), the yield of the product ($[Pd_6\mathbf{1}_8]^{12+}$), and the release rate of Py and compares them with the available experimental data.[3a] Although a very simple model was employed, the computational results showed a good agreement with the experimental results; moreover, the rapid consumption of $[PdPy_4]^{2+}$ and **1** at the early stage and the relatively slow production of $[Pd_6\mathbf{1}_8]^{12+}$ were observed. The consumption of $[PdPy_4]^{2+}$ and **1** and the release of Py were saturated around 180 min. On the other hand, the formation of the final product gradually started and was not accomplished even with a long time limit.

Next, we compared the computationally and experimentally obtained (n, k) values (Fig. 2e). Similar to the experimental ($\langle n\rangle$, $\langle k\rangle$) values, the computationally obtained ($n_{av}(t)$, $k_{av}(t)$) values were calculated based on the following equations.

$$n_{av}(t) = \frac{4a_{av}(t) - c_{av}(t)}{b_{av}(t)}, \quad k_{av}(t) = \frac{a_{av}(t)}{b_{av}(t)}$$

where a_{av}, b_{av}, and c_{av} are respectively given by,

$$a_{av}(t) = \langle N_{PdPy_4}(0)\rangle - \langle N_{PdPy_4}(t)\rangle - 6\langle N_{Pd_6\mathbf{1}_8}(t)\rangle$$

$$b_{av}(t) = \langle N_1(0)\rangle - \langle N_1(t)\rangle - 8\langle N_{Pd_6\mathbf{1}_8}(t)\rangle$$

$$b_{av}(t) = \langle N_{PdPy_4}(0)\rangle - 4\langle N_{PdPy_4}(t)\rangle - \langle N_{Py}(t)\rangle$$

As the time proceeds, n_{av} is monotonically increased with a slight decrease in k_{av} and finally (n_{av}, k_{av}) approaches (2.84, 0.75), which is very close to the values found for $[Pd_6\mathbf{1}_8Py]^{12+}$ (2.875, 0.75). The present computation successfully follows the trend except for the fact that the evolution in the computation is slightly slower than that observed experimentally.

Unlike the experimental n–k analysis, the present computation allows us to know the population of all the intermediates at any time; this is the biggest advantage of this computational approach. Fig. 3 shows the populations of the intermediates at six time slices: 0.01, 0.1, 1, 10, 50, and 100 min. This mapping makes the behavior of the observed (n, k) evolution clearer in terms of the underlying populations of each intermediate. For intermediate A: $Pd_a\mathbf{1}_bPy_c$, the (n_A, k_A) value namely, (n_A, k_A) = $((4a - c)/b, a/b)$ is represented by a circle, the size of which indicates its relative population. We discussed the time evolution of the intermediates towards the capsule *via* dividing

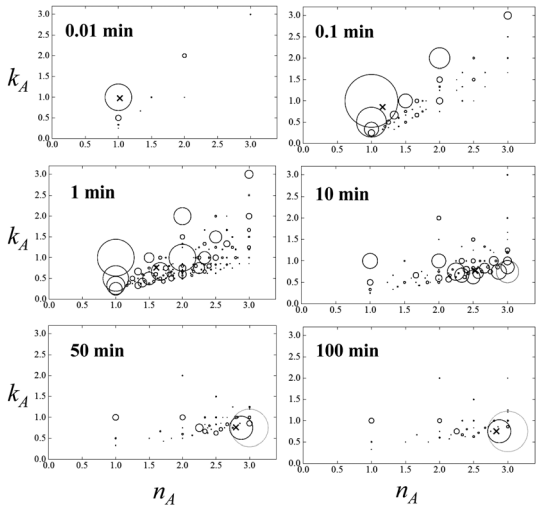

Fig. 3 The calculated distributions of the (n_A, k_A) values for the intermediate species. The (n_{av}, k_{av}) values are shown by the × mark. The dotted circles denote the distribution of the product. The area of circle proportional to $\langle N_A(t)\rangle$.

it into three stages (stage I: ~0.1 min, stage II: 0.1–10 min, and stage III: ~10 min).

Stage I: ~0.1 min

At 0.01 min, the main population appears at (1.0, 1.0) corresponding to two $[Pd\mathbf{1}Py_3]^{2+}$ generated from the simple ligand-exchange reaction of $[PdPy_4]^{2+}$ and **1**, and then, various species are distributed with time. A few populations at around n_A = 1.0 become larger at 0.1 min, indicating the production of $[Pd\mathbf{1}_2Py_2]^{2+}$ (k_A = 0.5) and $[Pd\mathbf{1}_3Py]^{2+}$ (k_A = 0.33) through further intermolecular ligand exchange reactions. In addition, the populations of $[Pd_2\mathbf{1}_2Py_5]^{4+}$ at (n_A, k_A) = (1.5, 1.0) and $[Pd_2\mathbf{1}Py_6]^{4+}$ at (n_A, k_A) = (2.0, 2.0) are relatively large, and other species such as $[Pd\mathbf{1}_4]^{2+}$, $[Pd_2\mathbf{1}_3Py_4]^{4+}$, and $[Pd_3\mathbf{1}_2Py_8]^{6+}$ are also populated. All the nine species, which are referred to as group I, are linear oligomers having only a few Pd–**1** bonds located near the reactant "010", as shown in Fig. 1.

Stage II: 0.1 min to 10 min

More various species were populated in stage II. In particular, the distribution at (n_A, k_A) = (2.0, 1.0) becomes larger at 1 min. The species whose (n, k) = (2.0, 1.0) are $[Pd_2\mathbf{1}_2Py_4]^{4+}$, $[Pd_3\mathbf{1}_3Py_6]^{6+}$, $[Pd_4\mathbf{1}_4Py_8]^{8+}$, $[Pd_5\mathbf{1}_5Py_{10}]^{10+}$, and $[Pd_6\mathbf{1}_6Py_{12}]^{12+}$; among these, $[Pd_2\mathbf{1}_2Py_4]^{4+}$ is dominant (above 90%). From 1 to 10 min, these distributions shift towards group II comprising 30 species mainly containing $[Pd_3\mathbf{1}_4Py_3]^{6+}$ at (n_A, k_A) = (2.25, 0.75), $[Pd_6\mathbf{1}_7Py_3]^{12+}$ at (3.0, 0.857), $[Pd_4\mathbf{1}_6Py_2]^{8+}$ at (2.33, 0.667), and $[Pd_5\mathbf{1}_8]^{10+}$ at (2.5, 0.625), which are located at the rightmost edge in each green enclosure shown in Fig. 1 and are produced by intramolecular ligand exchange with the release of Py.

Stage III: 10 min and longer

The capsule at (n_A, k_A) = (3.0, 0.75) was gradually populated after 10 min. Because the capsule is not an intermediate, this is excluded from the evaluation of (n_{av}, k_{av}). Thus, $[Pd_6\mathbf{1}_8Py]^{12+}$ at

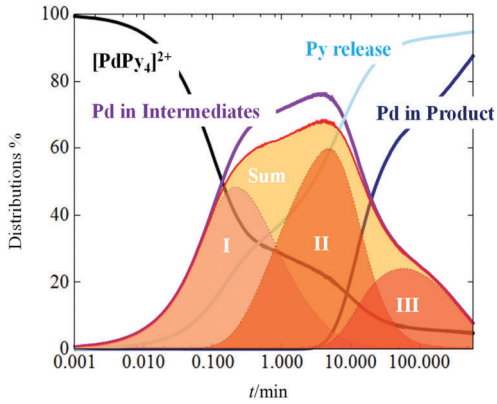

Fig. 4 The distribution of Pd in $[PdPy_4]^{2+}$, groups I–III, their sum, all of the intermediates and product. The distribution of released Py is also shown.

(2.875, 0.75) in group III is the main species, especially after 50 min or longer time region although small contributions from other intermediates still occur.

Fig. 4 displays a different view of the time evolution of the intermediates, showing the populations of Pd in the reactant ($[PdPy_4]^{2+}$), intermediates (groups I–III), and product ($[Pd_6\mathbf{1}_8]^{12+}$), together with the population of released Py. Within about 10 s, the reactants are rapidly converted into intermediates whose composition is intricately changed. Although groups I–III consist of only 40 species (about quarter of all the intermediates), the sum of groups I–III cover most of the distribution of Pd in the intermediates (by comparing the purple and red lines), indicating that these specific compounds play a dominative role in the self-assembly process. The released Py gradually increases with time. The final product starts to appear after approximately a few minutes and continuously increases with time longer time than 360 min.

The rapid consumption of the reactants to form group I and reactions among the species in group I are dominated by intermolecular Pd–**1** bond formation. The rate of the reaction should be proportional to the product concentrations of $[PdPy_4]^{2+}$ and **1**. At an early stage, the conversion proceeds quickly because of the relatively high concentration of these species. The production of these linear oligomers was followed by intramolecular Pd–**1** bond-formation with a gradual increase in Py release to produce the species of group II, in which the intramolecular ligand exchanges are no longer possible (Fig. 5). Thus, only the intermolecular processes were allowed to proceed for further self-assembly. However, because of decrease in the collision of the species and the backward Pd–**1** bond dissociation, the intermolecular ligand exchanges between the species in group II are slower than the intramolecular process; this makes the population of group II increase (from 1 to 10 min).

After the intermolecular ligand exchanges between species in group II, the intramolecular ligand exchanges in the resulting species produce group III or two conformational isomers of $[Pd_6\mathbf{1}_8Py]^{12+}$. Because of the significant difference in the activation energy from $[Pd_6\mathbf{1}_8Py]^{12+}$ to $[Pd_6\mathbf{1}_8]^{12+}$ in the two isomers, one of the two isomers was preferred to convert into the capsule, whereas the other isomer with a higher barrier acted as a kinetic trap. In fact, the slow production of $[Pd_6\mathbf{1}_8]^{12+}$ observed in the experiment

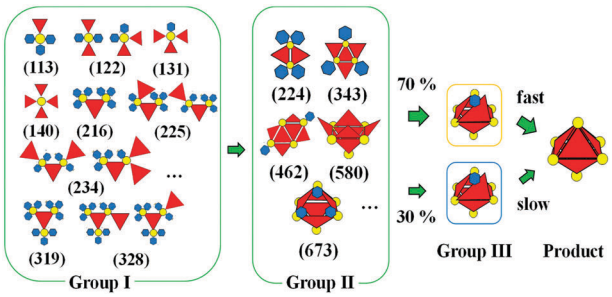

Fig. 5 Time evolution of the intermediates in the self-assembly of the $[Pd_6\mathbf{1}_8]^{12+}$ capsule.

could not be realized computationally only by assuming a slow conversion of a single isomer of $[Pd_6\mathbf{1}_8Py]^{12+}$, but was realized by considering this kinetic trap.

Conclusions

We constructed a reaction model to simply characterize the self-assembly process of the octahedron-shaped $[Pd_6\mathbf{1}_8]^{12+}$ capsules. The model was defined as a combination of several elementary reaction steps. The experimentally detected time evolution can be properly reproduced within a simple regime.[20] A computational approach utilizing the master equations for the elementary steps at a molecular level enables us to trace a long-time evolution of the process (second to hour or longer), which is far beyond the scope of the molecular dynamics simulations. The quantitative analysis of the distributions of all the intermediates was performed, which could not be obtained only by the experimental *n*–*k* analysis. Although the self-assembly process of the octahedron-shaped $[Pd_6\mathbf{1}_8]^{12+}$ capsule was quite complicated, taking place through several pathways, the characterization of the dominant intermediates was possible: linear oligomers with a few Pd–**1** bonds at the initial stage, intramolecular Pd–**1** bonds saturated at the middle stage, and kinetic trapping state $[Pd_6\mathbf{1}_8Py]^{12+}$ at the final stage. These characteristics of cage formation reminds us of protein folding processes.[21]

The simple description of the process before the final step is expected to be reasonable enough, where the complicated and reversible self-assembly pathways can avoid a high barrier route and easily make intermediates well mix, rapidly converge into some dominant types. On the other hand, the elaborated treatment of $[Pd_6\mathbf{1}_8Py]^{12+}$ is necessary because all the pathways have to go through this composition as a final step. The rigidity of this almost completed cluster limits the reversible process such as the fast escape from kinetic trapping. Because the experiment of the self-assembly of the $[Pd_6\mathbf{1}_{18}]^{12+}$ capsule has been performed at room temperature (298 K), the contribution from this kinetic trapping may become smaller as the temperature increases.

Acknowledgements

The work was financially supported by MEXT KAKENHI (Grant Numbers JP25102001, JP25102002, JP25102005, and JP15K21708),

the 'Elements Strategy Initiative for Catalysts & Batteries (ESICB)', the and Asahi Glass Foundation. One of the authors (Y. M.) thanks the Grant-in Aid for the JSPS Fellowship.

Notes and references

1 (*a*) G. M. Whitesides and B. Grzybowski, *Science*, 2002, **295**, 2418; (*b*) G. M. Whitesides and M. Boncheva, *Proc. Natl. Acad. Sci. U. S. A.*, 2002, **99**, 4771.
2 *Molecular Self-Assembly: Advances and Applications*, ed. A. D. Q. Li, Pan Stanford Publishing, 2013.
3 (*a*) Y. Tsujimoto, T. Kojima and S. Hiraoka, *Chem. Sci.*, 2014, **5**, 4167; (*b*) S. Hiraoka, *Chem. Rec.*, 2015, **15**, 1144; (*c*) S. Hiraoka, K. Harano, M. Shiro, Y. Ozawa, N. Yasuda, K. Toriumi and M. Shionoya, *Angew. Chem.*, 2006, **118**, 6638.
4 T. R. Cook, Y.-R. Zheng and P. J. Stang, *Chem. Rev.*, 2013, **113**, 734.
5 M. Fujita, *Chem. Soc. Rev.*, 1998, **27**, 417.
6 M. F. Hagan and D. Chandler, *Biophys. J.*, 2006, **91**, 42.
7 D. C. Rapaport, *Phys. Biol.*, 2010, **7**, 045001.
8 (*a*) M. Yoneya, T. Yamaguchi, S. Sato and M. J. Fujita, *Am. Chem. Soc.*, 2012, **134**, 14401; (*b*) M. Yoneya, S. Tsuzuki, T. Yamaguchi, S. Sato and M. Fujita, *ACS Nano*, 2014, **8**, 1290.
9 D. T. Gillespie, *Ann. Rev. Phys. Chem.*, 2007, **58**, 35.
10 (*a*) M. R. D'Orsogna, G. Lakatos and T. J. Chou, *Chem. Phys.*, 2012, **136**, 084110; (*b*) M. R. D'Orsogna, B. Zhao, B. Berenji and T. J. Chou, *Chem. Phys.*, 2013, **139**, 121918.
11 A. B. Bortz, M. H. Kalos and J. L. Lebowitz, *J. Comput. Phys.*, 1975, **17**, 10.
12 R. E. Glaser, M. A. Delarosa, A. O. Salau and C. J. Chicone, *Chem. Educ.*, 2014, **91**, 1009.
13 T. B. Kepler and T. C. Elston, *Biophys. J.*, 2001, **81**, 3116.
14 W. S. Hlavacek, A. Remondo, C. Wofsy and B. Goldstein, *Bull. Math. Biol.*, 2002, **64**, 887.
15 H. Qian and L. M. Bishop, *Int. J. Mol. Sci.*, 2010, **11**, 3472.
16 J. A. Miller and S. J. J. Klippenstein, *Phys. Chem. A*, 2006, **110**, 10528.
17 M. J. Pilling and S. H. Robertson, *Ann. Rev. Phys. Chem.*, 2003, **54**, 245.
18 (*a*) A. J. Zlotnick, *Mol. Recognit.*, 2005, **18**, 479; (*b*) P. Moisant, H. Neeman and A. Zlotnick, *Biophys. J.*, 2010, **99**, 1350; (*c*) D. Endres, M. Miyahara, P. Moisant and A. Zlotnick, *Protein Sci.*, 2005, **14**, 1518.
19 (*a*) B. Sweeney, T. Zhang and R. Schwartz, *Biophys. J.*, 2008, **94**, 772; (*b*) T. Zhang, R. Rohlfs and R. Schwartz, Proceedings of the 2005 Winter Simulation Conference, Orlando, 2005, p. 2223.
20 The self-assembly system using another tritopic ligand, **2**, can also be described using the same reaction model framework as summarized in ESI†.
21 S. W. Englander and L. Mayne, *Proc. Natl. Acad. Sci. U. S. A.*, 2014, **111**, 15873.

